Article

Lagrangian Drifter to Identify Ocean Eddy Characteristics

Peter C. Chu*, Chenwu Fan

Naval Postgraduate School, pcchu@nps.edu; fan@nps.edu
* Correspondence: pcchu@nps.edu

Abstract: Deterministic-stochastic empirical mode decomposition (EMD) is used to obtain low-frequency (non-diffusive, i.e., background velocity) and high-frequency (diffusive, i.e., eddies) components from a Lagrangian drifter's trajectory. Eddy characteristics are determined from the time series of eddy trajectories from individual Lagrangian drifter such as the eddy radial scale, eddy velocity scale, eddy Rossby number, and eddy-background kinetic energy ratio. A long-term dataset of the SOund Fixing And Ranging float time series obtained near the California coast by the Naval Postgraduate School from 1992 to 2004 at depth between 150 and 600 m (http://www.oc.nps.edu/npsRAFOS/) is used as an example to demonstrate the capability of the deterministic-stochastic EMD.

Keywords: Lagrangian drifter; RAFOS floats; empirical mode decomposition (EMD); deterministic-stochastic EMD; intrinsic mode function (IMF); eddy radial scale; eddy velocity scale; eddy Rossby number; eddy-current kinetic energy ratio

---

1. Introduction

A Lagrangian trajectory $\mathbf{x}(t)$ can be separated into deterministic [low frequency mode representing the background trajectory $\mathbf{x}_b(t)$] and stochastic [non-low frequency mode representing eddy trajectory, $\mathbf{x}_{eddy}(t)$],

$$\mathbf{x}(t) = \mathbf{x}_b(t) + \mathbf{x}_{eddy}(t) \tag{1}$$

using the empirical mode decomposition (EMD) with the steepest ascending mode ratio, called the *deterministic-stochastic EMD* [1] and wavelet decomposition [2]. Here, $\mathbf{x}(t)$ is the position vector at time t. The Lagrangian velocity is calculated by

$$\mathbf{u} = \frac{d\mathbf{x}(t)}{dt},\quad \mathbf{u}_b = \frac{d\mathbf{x}_b(t)}{dt},\quad \mathbf{u}_{eddy} = \frac{d\mathbf{x}_{eddy}(t)}{dt}. \tag{2}$$

Such Lagrangian-type decomposition changes the traditional approach of using N drifters [$\mathbf{x}^{(n)}(t)$, n = 1, , …, N] to get background velocity (i.e., mean flow) and eddies from Lagrangian trajectory data, i.e., the background velocity is the Eulerian mean from the N drifters,

$$\mathbf{U}(x, y, t) = \left\langle \left[\mathbf{u}^{(n)}(t) \right] \right\rangle, \tag{3}$$

and subtraction of $\mathbf{U}$ from the observed Lagrangian drifters leads to the "residue" velocities,

$$\mathbf{u}^{(n)}{}'(x, y, t) = \frac{d\mathbf{x}^{(n)}(t)}{dt} - \mathbf{U}(x, y, t), \tag{4}$$

is taken as the eddy velocity. Here, the bracket represents an ensemble average in the defined geographic region. The velocities are calculated from Lagrangian trajectories using binned velocities with cubic splines [3], routine ocean data assimilation systems [4] and data analysis methods such as optimal interpolation [5], and optimal spectral decomposition (OSD) [6, 7]. A formula was derived to link the Eulerian velocity at grid points to the Lagrangian trajectory [8]. Obviously, $\mathbf{u}^{(n)}{}'(x, y, t)$ is not the same as $\mathbf{u}^{(n)}_{eddy}(t)$.

The trajectories of 54 SOund Fixing And Ranging (RAFOS) floats deployed near California coast by C.A. Collins of the Naval Postgraduate School from 1992 to 2004 at depth between 150 and 600 m (http://www.oc.nps.edu/npsRAFOS/DATAS/) (Figure 1) show combination of deterministic (low frequency) and stochastic (high frequency) components. The first SOFAR floats sent out pings that were picked up by fixed stations; RAFOS floats revered that, and listened to pings sent out from the fixed stations. The traditional approach needs large number (N) of drifters to get statistically meaningful $\mathbf{U}(x, y, t)$. What should we do if there is no sufficient number of drifters co-deployed? For example, there were usually less than three RAFOS floats were available at same time-periods by the Naval Postgraduate School (NPS) (see website: http://www.oc.nps.edu/npsRAFOS/DATAS/).

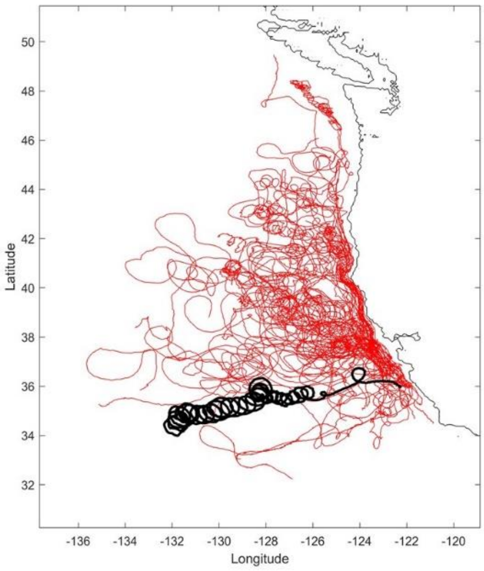

Figure 1. Trajectories of 54 RAFOS floats in the California coast by the Naval Postgraduate School between 1992 and 2004 (http://www.oc.nps.edu/npsRAFOS/). The thick black trajectory refers to the Float N073.

An alternative approach is to use the deterministic-stochastic EMD (1) to separate background velocity and eddies from a single Lagrangian drift. After the separation, the background velocity scale as well as eddy characteristic parameters such as the eddy radial scale, eddy velocity scale, eddy Rossby number, and eddy-background kinetic energy ratio can be identified. The rest of the paper is organized as follows. Section 2 describes the procedure of the deterministic-stochastic EMD. Section 3 and 4 present the identified background velocity and eddy characteristic parameters for each RAFOS

Preprints (www.preprints.org) | NOT PEER-REVIEWED | Posted: 19 October 2019 doi:10.20944/preprints201910.0227.v1

Peer-reviewed version available at Climate 2019, 7, 137; doi:10.3390/cli7120137

float and their statistics for 54 RAFOS floats. Section 5 describes the temporal variability of the background and eddy characteristic parameters. Section 6 presents the results.

2. Deterministic-stochastic EMD

The EMD decomposes a Lagrangian trajectory into intrinsic mode functions (IMFs) regardless of their linearity, stationarity, and stochasticity [9-11]. It was also used to separate the oceanic wave motion from turbulence [12]. The key point to perform this decomposition is the sifting process with four steps, which decompose a Lagrangian drift trajectory $\mathbf{x}(t)$ into

$$\mathbf{x}(t) = \sum_{p=1}^{P} \mathbf{x}_p(t) + \mathbf{r}(t) \quad (5)$$

where $\mathbf{x}_p(t) = [x_p(t), y_p(t)]$, is the p-th IMF and $\mathbf{r}(t) = [r_x(t), r_y(t)]$ is the trend (not oscillated). The first IMF has highest frequency, and frequency reduces as the subscript p increases. The trajectory data of RAFOS float #N073 from http://www.oc.nps.edu/npsRAFOS/DATAS/NPS035/DATAS.html is used as an illustration and represented as a thick curve in Figure 1. The data are time series of horizontal positon vector, $\mathbf{x}(t_i) = [x(t_i), y(t_i)]$, with x in the zonal direction, and y in the latitudinal direction [13, 14].

The RAFOS subsurface data downloaded from http://www.oc.nps.edu/npsRAFOS/DATAS/ contains 61 RAFOS floats. Among them 7 floats (N001, N009, N012, N042, N046, N049, N068) have too many missing data inside the time series. They are not included in the computation. The date rate varies from general 3/day to around 22/day (N030 18 May – 10 June 1994). For each float, the time series $[x(t_i), y(t_i)]$ are decomposed into IMFs and trend using the EMD method [9]. Seven IFMs and a trend are identified in the (x, y) directions (Figure 2). It clearly shows that the high frequency motion dominates the low IFM modes. Frequency reduces as the IFM mode from the lowest (IMF-1) to the highest (IMF-7). The trend (no oscillation) is of course the part of the deterministic motion, but not all.

The IMFs are separated into two additive components, deterministic and stochastic, using the steepest ascent low/non-low frequency ratio [1]. For RAFOS N073, combination of IMF-1 to IMF-4 is the high-frequency component (eddy) and combination of IMF-5 to IMF-7 and the trend is the low-frequency component (i.e., mean flow). After the separation of Lagrangian drifter‘s trajectory into deterministic and stochastic components with the total number of position points of J,

$$x(t_j) = x_{det}(t_j) + x_{sto}(t_j), \quad y(t_j) = y_{det}(t_j) + y_{sto}(t_j), \quad j = 1, 2, ..., J \quad (6)$$

the deterministic and stochastic velocities can be calculated from position vector (only showing x-direction) with the first-order difference for the two end points,

$$u_{sto}(t_1) = \frac{x_{sto}(t_2) - x_{sto}(t_1)}{t_2 - t_1}, \quad u_{sto}(t_J) = \frac{x_{sto}(t_J) - x_{sto}(t_{J-1})}{t_J - t_{J-1}} \quad (7)$$

and the central difference for the internal points,

$$u_{sto}(t_j) = \frac{x_{sto}(t_{j+1}) - x_{sto}(t_{j-1})}{t_{j+1} - t_{j-1}}, \quad j = 2, 3, ..., J\text{-}1 \quad (8)$$

Preprints (www.preprints.org) | NOT PEER-REVIEWED | Posted: 19 October 2019 doi:10.20944/preprints201910.0227.v1

Peer-reviewed version available at *Climate* **2019**, *7*, 137; doi:10.3390/cli7120137

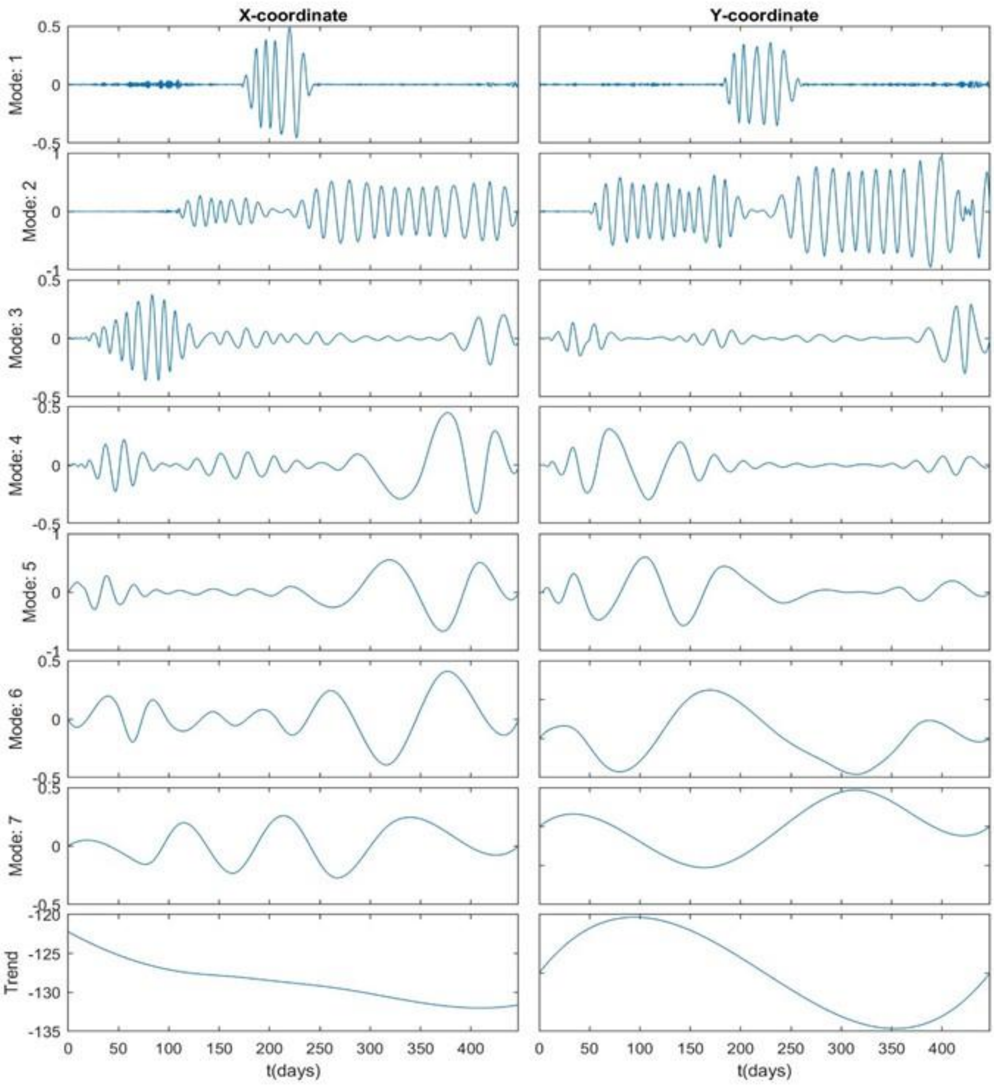

Figure 2. The IMFs and trend of (a) x(t) and (b) y(t) of the RAFOS float N073 from 21 November 1999 to 12 February 2001. Combination of IMF-1 to IMF-4 is the high-frequency component (eddy) and combination of IMF-5 to IMF-7 and the trend is the low-frequency component (i.e., mean flow).

Figure 3 shows the observed (red), deterministic (blue), and stochastic (green) trajectories of RAFOS N073. The deterministic trajectory represents the background velocity. The stochastic trajectory indicates the eddy. The eddy is transported along the deterministic trajectory. The eddy in Figure 3 does not represent its real position and is separated from the deterministic trajectory arbitrarily just for illustration of eddy-like motion.

Preprints (www.preprints.org) | NOT PEER-REVIEWED | Posted: 19 October 2019 doi:10.20944/preprints201910.0227.v1

Peer-reviewed version available at Climate 2019, 7, 137; doi:10.3390/cli7120137

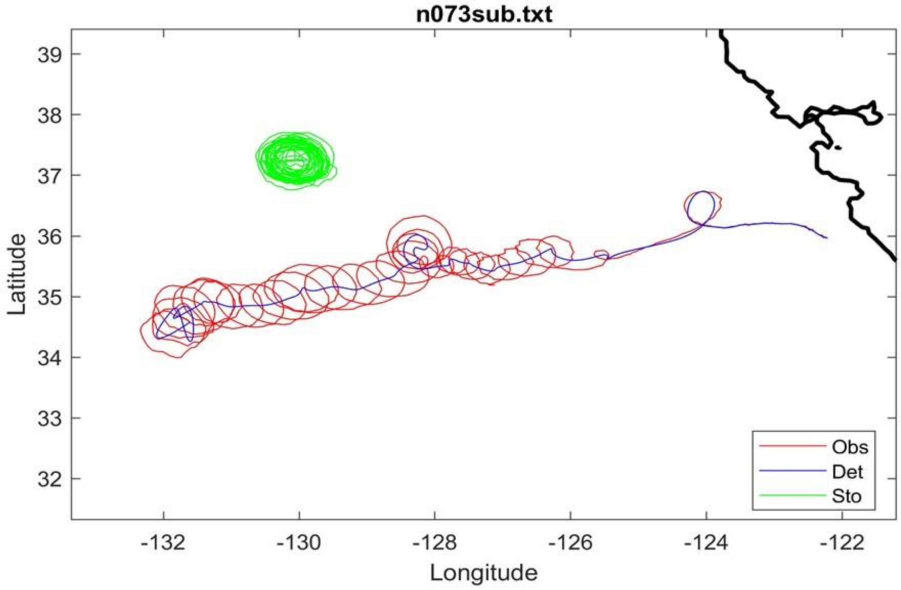

Figure 3. Observed (red), deterministic (blue), and stochastic (green) trajectories of RAFOS N073. The deterministic trajectory represents the mean flow. The stochastic trajectory indicates the eddy. The center of the eddy is transported by the mean flow (i.e., along the deterministic trajectory), and is put away from the deterministic trajectory arbitrarily just for illustration of eddy-like motion.

3. Eddy characteristics identified from an individual RAFOS float

After the deterministic and stochastic trajectories and velocities are obtained from an individual RAFOS float, the eddy characteristics can be easily identified during the float's drifting period. The eddy radial scale is defined by the root mean square of the stochastic trajectory

$$L_{eddy} = \sqrt{\frac{1}{J}\left[\sum_{j=1}^{J}\left\{\left[x_{sto}^2(t_j) + y_{sto}^2(t_j)\right]\right\}\right]} \tag{9}$$

The eddy velocity scale (V_{eddy}) is defined by

$$V_{eddy} = \sqrt{\left[\frac{1}{J}\sum_{j=1}^{J}\left\{\left[\left(\frac{dx_{sto}(t_j)}{dt}\right)^2 + \left(\frac{dy_{sto}(t_j)}{dt}\right)^2\right]\right\}\right]} \tag{10}$$

The eddy kinetic energy per unit mass (E), eddy angular velocity scale (Ω_{eddy}), and eddy Rossby number (R_{eddy}) are defined by

$$E_{eddy} = \frac{V_{eddy}^2}{2}, \quad \Omega_{eddy} = \frac{V_{eddy}}{L_{eddy}}, \quad R_{eddy} \equiv \frac{V_{eddy}}{fL_{eddy}} = \frac{\Omega_{eddy}}{f}, \tag{11}$$

where f is the Coriolis parameter, which is evaluated at 40°N here. The background velocity (treated as current velocity) scale (V_b) is defined by

$$V_b = \sqrt{\frac{1}{J}\sum_{j=1}^{J}\left\{\left[\left(\frac{dx_{det}(t_j)}{dt}\right)^2 + \left(\frac{dy_{det}(t_j)}{dt}\right)^2\right]\right\}} \tag{12}$$

Peer-reviewed version available at Climate 2019, 7, 137; doi:10.3390/cli7120137

The background kinetic energy per unit mass (E_b) and the eddy/background kinetic energy ratio (r) are defined by

$$E_b = \frac{V_b^2}{2}, \quad r = \frac{E_{eddy}}{E_b} = \frac{V_{eddy}^2}{V_b^2} \tag{13}$$

Due to eddy's circular motion (green trajectory in Figure 3), the time series of $[x_{sto}(t_j), v_{sto}(t_j)]$ or $[y_{sto}(t_j), u_{sto}(t_j)]$ determine the types of eddy (cylcynic or anticyclonic),

$$x_{sto}(t_j) > 0 \rightarrow \begin{cases} v_{sto}(t_j) > 0 \rightarrow \text{cyclonic} \\ v_{sto}(t_j) < 0 \rightarrow \text{anticyclonic} \end{cases}$$
$$x_{sto}(t_j) < 0 \rightarrow \begin{cases} v_{sto}(t_j) > 0 \rightarrow \text{anticyclonic} \\ v_{sto}(t_j) < 0 \rightarrow \text{cyclonic} \end{cases} \tag{14}$$

Table 1 shows the eddy-current kinetic energy ratio (r) as well as the number of cyclonic/anticylonic spirals. For the RAFOS float N073 float, we have

$$27 \text{ anticyclonic spirals}, \quad r = 5.45 \tag{15}$$

Altogether, we identified 36 cyclonic (denoted by 'C') eddies and 203 anticyclonic (denoted by AC) eddies from 54 RAFOS floats.

4. Statistics of eddy characteristic parameters

Histograms of the background velocity scale (V_b) and eddy characteristic parameters such as radial scale (L_{eddy}), velocity scale (V_{eddy}), Rossby number (R_{eddy}), and eddy-background kinetic energy ratio (r) are constructed from 54 RAFOS floats. All the histograms are non-symmetric, high dispersive, and positively skewed (Figure 4). The overall eddy kinetic energy is more than the background kinetic energy with the E_{eddy}/E_b ratio having the mean of 1.78, the standard deviation of 2.00, the skewness of 2.79, and the kurtosis 12.00 (Table 2). The eddy radial scale (L_{eddy}) has a mean of 18.37 km, minimum of 1.12 km, maximum of 102.21 km, standard deviation of 21.33 km, skewness of 2.31, and kurtosis of 8.50. The eddy velocity scale has a mean of 11.98 cm/s, minimum of 2.72 cm/s, maximum of 44.17 cm/s, standard deviation of 8.65 cm/s, skewness of 1.74, and kurtosis of 5.82.

Preprints (www.preprints.org) | NOT PEER-REVIEWED | Posted: 19 October 2019 doi:10.20944/preprints201910.0227.v1

Peer-reviewed version available at *Climate* **2019**, *7*, 137; doi:10.3390/cli7120137

Table 1. Identified 36 cyclonic (denoted by 'C') spirals and 203 anticyclonic (denoted by AC) spirals and eddy to current kinetic energy ratio from 54 RAFOS floats.

Float	Buoy Days	dbar	# spirals	r	Float	Buoy Days	dbar	# spirals	r
N002	8/12-9/11/92	350	C: 1	2.57	N050	8/29/96-1/9/98	275	AC: 1	1.08
N003	8/12-9/11/92	350	AC: 1	1.27	N051	2/25/97-7/8/98	275	AC: 3	1.91
N004	7/07-9/05/93	350	AC: 3	1.01	N053	9/11/97-8/22/98	275	C: 5	2.03
N005	9/03/93-1/01/94	350	AC: 2	1.70	N055	9/11/97-8/22/98	275	AC: 1	0.52
N006	11/20/93-5/02/94	350	AC: 2	1.71	N062	4/29/98-6/25/99	275	AC: 9	0.50
N007	7/07-9/05/93	350	AC: 5	0.13	N063	5/17/98-7/12/99	275	AC: 4	0.66
N008	9/3-12/30/93	350	AC: 2	1.09	N064	4/29/98-6/25/99	275	AC: 8	1.67
N010	9/3/93-1/1/04	350	C: 1	0.76	N065	4/29/98-6/24/99	275	C: 2	3.94
N011	11/20/93-3/2/94	350	AC: 3	2.03	N066	10/27/98-12/23/99	275	C: 6	0.66
N013	11/20/93-3/2/94	350	AC: 2	1.94	N067	10/27/98-12/23/99	275	AC:11	3.01
N014	1/11-4/23/94	350	C: 1	1.39	N069	5/5/99-5/18/00	275	AC: 1	0.63
N019	4/25-11/11/94	275	AC: 5	1.64	N071	5/5/99-5/18/00	275	AC: 5	0.95
N021	5/19-6/10/94	275	AC: 1	1.96	N072	11/21/99-2/12/01	275	AC: 7	1.30
N022	5/19-6/10/94	275	AC: 3	4.20	N073	11/21/99-2/12/01	275	AC: 27	5.45
N024	5/17-6/9/94	275	AC: 5	11.18	N075	11/21/99-2/12/01	275	C: 1	0.20
N026	8/22-12/30/94	290	AC: 3	0.71	N080	7/26/00-9/23/01	275	AC:10	0.52
N028	8/12-12/19/94	350	AC: 5	2.38	N081	7/26/00-5/22/02	275	AC: 2	0.72
N029	10/25/95-6/28/96	300	AC: 1	1.65	N082	7/26/00-9/24/01	275	C: 4	0.59
N030	5/18-6/10/94	275	AC: 1	5.59	N083	9/11/00-12/29/01	275	AC: 9	3.18
N031	8/22-12/30/94	290	AC: 4	8.13	N084	9/11/00-7/9/02	275	C: 1	0.23
N032	8/7/95-10/6/96	300	C: 4	1.61	N085	9/11/00-7/9/02	275	AC: 5	0.40
N033	8/12/94-5/10/95	350	AC: 5	0.48	N087	5/20/01-11/6/02	275	C: 1	0.56
N035	8/7/95-11/5/96	300	C: 1	0.31	N088	5/20/01-7/28/03	275	AC: 5	1.19
N039	7/29/96-12/10/97	275	AC: 3	0.36	N089	5/20/01-7/28/03	275	AC: 4	1.19
N041	7/29/96-11/17/97	275	C: 1	2.70	N090	12/6/01-3/9/04	275	AC: 6	1.65
N043	2/25-12/13/97	275	AC: 3	1.26	N091	12/5/01-3/9/04	275	AC: 8	0.18
N048	7/29/96-9/19/97	275	C: 1	1.08	N092	12/5/01-3/9/04	275	C: 6	0.43

Table 2. Statistics of the eddy parameters identified from 54 RAFOS floats (1992-2004).

Parameter	Mean	Min	Max	Standard Deviation	Skewness	Kurtosis
L_{eddy} (km)	18.37	1.12	102.21	21.33	2.31	8.50
V_{eddy} (cm/s)	11.98	2.72	44.17	8.65	1.74	5.82
V_b (cm/s)	10.04	4.19	31.59	5.39	2.38	8.96
R_{eddy}	0.35	0.01	3.99	0.86	3.34	12.90
r	1.78	0.13	11.19	2.00	2.79	12.00

Preprints (www.preprints.org) | NOT PEER-REVIEWED | Posted: 19 October 2019 doi:10.20944/preprints201910.0227.v1

Peer-reviewed version available at *Climate* **2019**, *7*, 137; doi:10.3390/cli7120137

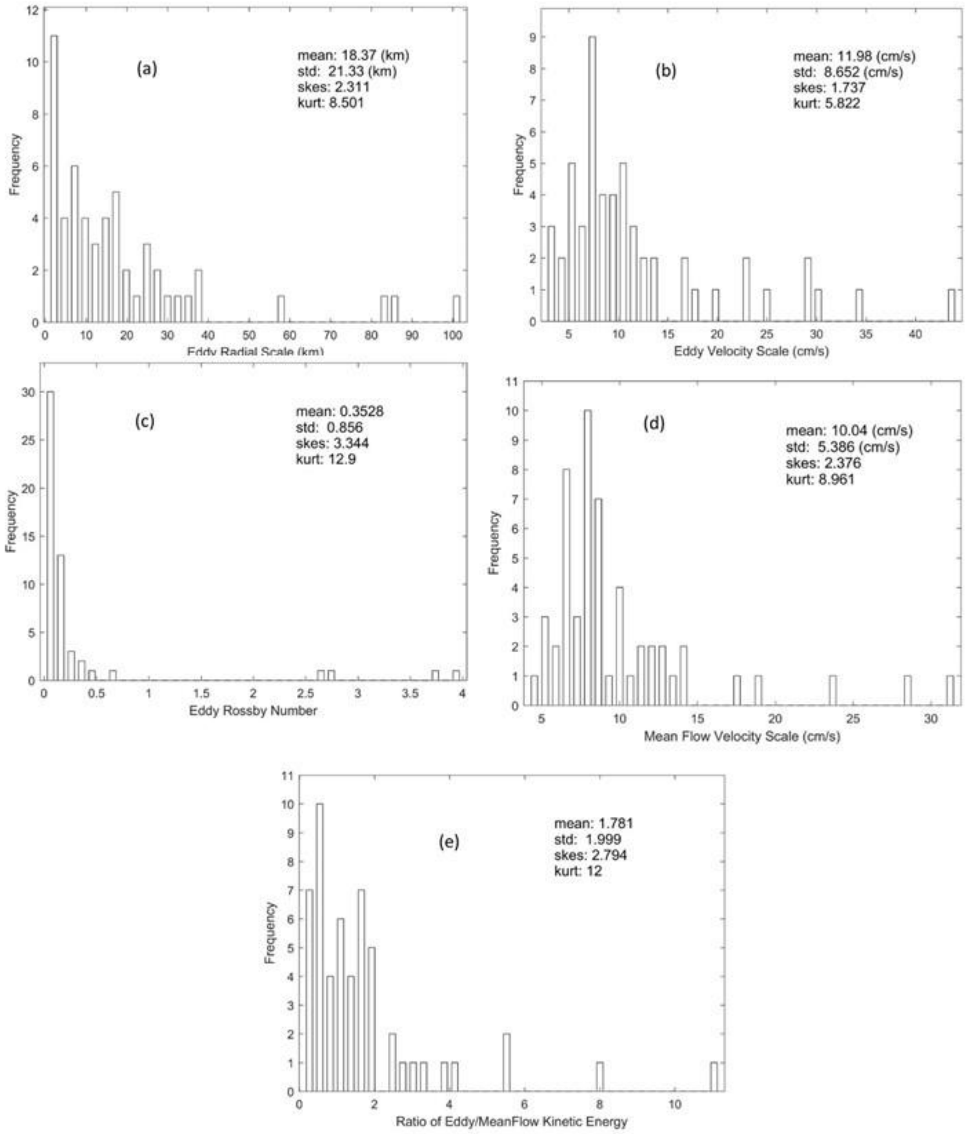

Figure 4. Histograms of current and eddy characteristic parameters identified from 54 RAFOS floats: (a) eddy radial scale (km), (b) eddy velocity scale (cm/s), and (c) eddy Rossby number, (d) current velocity scale (cm/s), and (e) eddy and current kinetic energy ratio.

5. Temporal variability of eddy characteristic parameters

All the identified eddy and background parameters (L_{eddy}, V_{eddy}, R_{eddy}, V_b, r) have evident temporal variabilities (Figure 5). Large dispersion is found in L_{eddy} before August 1998 from 1.12 km (7 July – 5 September 1993, N007) to 102.21 km (25 February 1997 – 8 July 1998, N051). Small dispersion in L_{eddy} is found after August 1998 with a maximum of 36.53 km (21 November 1999 – 12 February 2001, N073) (Figure 5a) and a minimum of 1.81 km (5 May 1999 – 18 May 2000, N069). There was a strong El Nino and Southern Oscillation (ENSO) event in the North Pacific in 1997-1998. The effect of ENSO needs to be further investigated.

doi:10.20944/preprints201910.0227.v1

Peer-reviewed version available at Climate 2019, 7, 137; doi:10.3390/cli7120137

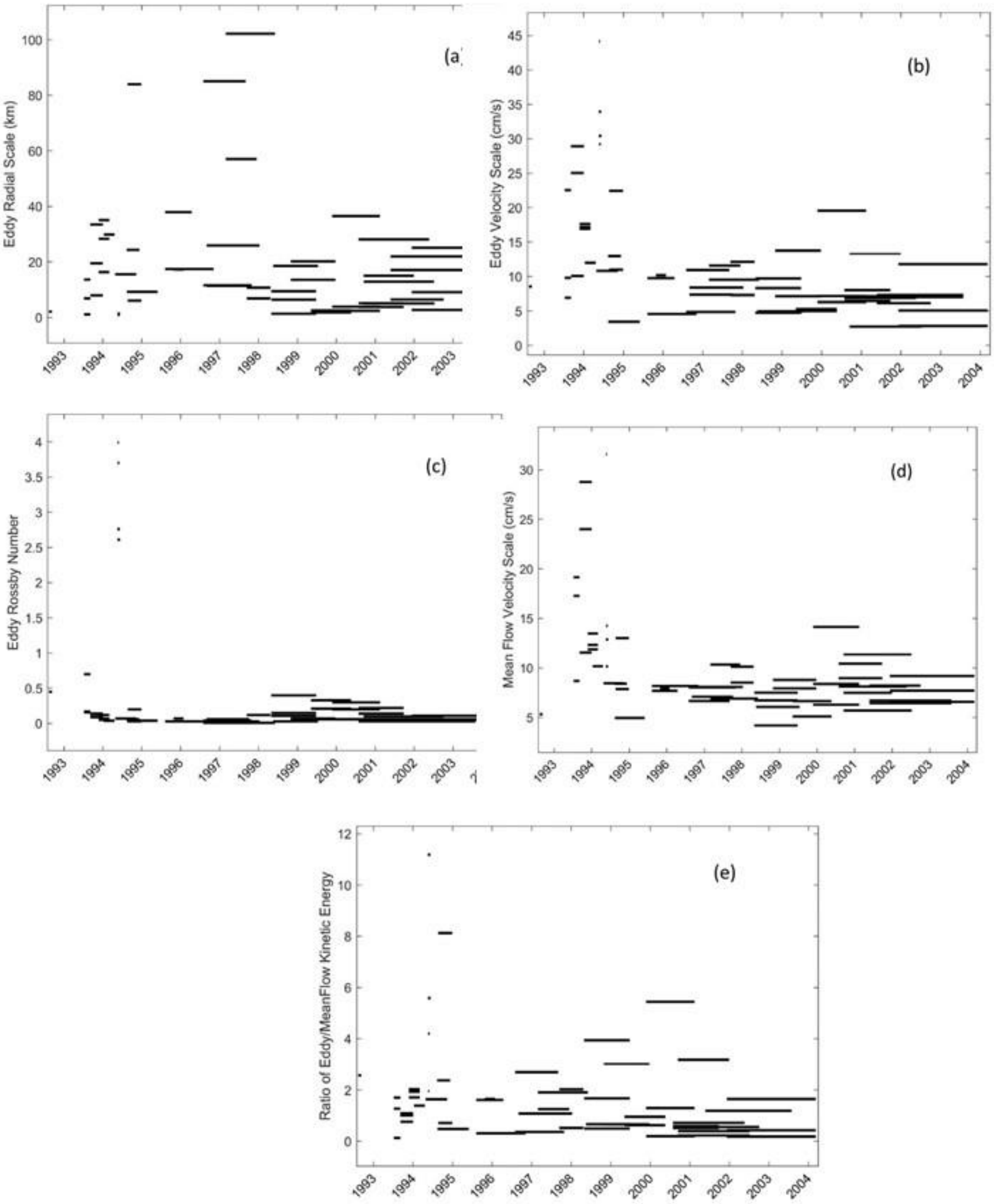

Figure 5. Temporal variation of identified current and eddy characteristic parameters from 54 RAFOS floats: (a) eddy radial scale (km), (b) eddy velocity scale (cm/s), and (c) eddy Rossby number, (d) current velocity scale (cm/s), and (e) eddy and current kinetic energy ratio.

Large dispersion is found in V_{eddy} before 1995 from 6.91 cm/s (7 July – 5 September 1993, N007) to 44.17 cm/s (19 May –10 June 1994, N021). Small dispersion is found after December 1994 with a maximum of 19.56 cm/s (21 November 1999 – 12 February 2001, N073) and a minimum of 2.72 cm/s (11 September 2000 – 9 July 2002, N084) (Figure 5b). The eddy Rossby number (R_{eddy}) is mostly less than 0.5 (Figure 5c). Large disperse is found before 1995 with large values of 3.99 (N021), 3.70 (N022), 2.76 (N024), during 17 May – 10 June 1994 and 18 May-10 June 1994 and small value of 0.03 during 7 August – 30 December 1994 (N031). Small dispersion is found after 1995 with a maximum of 0.33 during 5 May 1999 - 18 May 2000 (N069) (Figure 5c). The background velocity scale (V_b) has larger dispersion before 1995. It has a maximum of 31.59 cm/s during 19 May – 10 June 1994 (N021) and a minimum of 5.33 cm/s during 12 August – 11 September 1992 (N002). It has smaller dispersion

Preprints (www.preprints.org) | NOT PEER-REVIEWED | Posted: 19 October 2019 doi:10.20944/preprints201910.0227.v1

Peer-reviewed version available at *Climate* **2019**, *7*, 137; doi:10.3390/cli7120137

after 1995 with a maximum of 14.14 cm/s during 21 November 1999 – 12 February 2001 (N075) and a minimum of 4.19 cm/s during 29 April 1998 – 24 June 1999 (N065) (Figure 5d). The E_{eddy}/E_b ratio has larger dispersion before 1995 with a maximum of 11.18 during 17 May – 9 June 1994 (N024) and a minimum of 0.13 during 7 July – 5 September 1993 (N007). It has smaller dispersion after 1995 with a maximum of 5.45 during 21 November 1999 – 12 February 2001 (N073) and a minimum of 0.23 values during 11 September 2000 – 9 July 2002 (N084) (Figure 5e).

6. Conclusions

The deterministic-stochastic EMD is used to decompose a Lagragian trajectory. Time differentiation of the deterministic and stochastic trajectories leads to the Lagragian background and eddy velocities. Five parameters can be identified from a single Lagrangian drifter data to represent background velocity and eddy characteristics such as the eddy radial scale (L_{eddy}), eddy velocity scale (V_{eddy}), eddy Rossby number (R_{eddy}), background velocity scale (V_b), and eddy-background kinetic energy ratio (r).

The NPS RAFOS dataset consisting of 54 floats is used as an example to demonstrate the capability of the deterministic-stochastic EMD. The obtained 54 sets of parameters (L_{eddy}, V_{eddy}, R_{eddy}, V_b, r) show an eddy-rich area near the California coast with the mean eddy-background kinetic energy ratio of 1.78. These eddies are mostly anticylconic with total 203 anticyclonic and 36 cyclonic spirals. Both submesoscale and mesoscale eddies exist with the mean eddy Rossby number of 0.72 for the submesoscale eddies and 0.06 for the mesoscale eddies. The overall eddy velocity scales are comparable between the submesoscale eddies (mean: 11.35 cm/s) and the mesoscale eddies (mean: 12.49 cm/s). The background-eddy kinetic energy transfer is similar between the two. The identified eddy characteristic parameters have evident temporal variabilities. Large dispersion is found in L_{eddy} before August 1998 and small dispersion in L_{eddy} is found after August 1998. However, large dispersion of (V_{eddy}, R_{eddy}, V_b, r) is found before 1995 and small dispersion is found after 1995. Further studies are needed on physical mechanisms to cause such a temporal variability, especially the ENSO effect.

Author Contributions: conceptualization, P.C.; methodology, P.C.; software, C.F.; validation, C.F.; formal analysis, P.C.; investigation, C.F.; resources, P.C.; data curation, C.F.; writing—original draft preparation, P.C.; writing—review and editing, P.C.; visualization, C.F.; supervision, P.C.; project administration, P.C..

Funding: This research received no external funding.

Acknowledgments: The authors would like to thank Professor (emeritus) Curt Collins at the Naval Postgraduate School for collecting RAFOS data and unselfishly providing data at the website.

Conflicts of Interest: The authors declare no conflict of interest.

References

1. Chu, P.C. Steepest ascent low/non-low frequency ratio in empirical mode decomposition to separate deterministic and stochastic velocities from a single Lagrangian drifter. *J. Geophys. Res. Oceans* 2019, **123**, 1708-1721.
2. Ivanov, L.M.; Chu, P.C. Estimation of turbulent diffusion coefficients from decomposition of Lagragian trajectories. Ocean Modelling 2019, 137, 114-131.
3. Bauer, S.; Swenson, M. S.; Griffa, A.; Mariano, A. J.; Owens, K. Eddy-mean decomposition and eddy-diffusivity estimates in the tropical Pacific Ocean. *J. Geophys. Res. Oceans* 1998 **103**, 30,855–30,871.
4. Galanis, G.N.; Louka, P.; Katsafados, K. P.G.; Pytharoulis, I. Applications of Kalman filters based on non-linear functions to numerical weather predictions. *Ann. Geophys.* 2006, **24**, 2451-2460.
5. Lozano, C. J.; Robinson, A. R.; Arrango, H. G.; Gangopadhyay, A.; Sloan, Q.; Haley, P. J.; Anderson, L.; Leslie, W. An interdisciplinary ocean prediction system: Assimilation strategies and structured data models. Modern Approaches to Data Assimilation in Ocean Modeling, P. Malanotte-Rizzoli, Ed., Elsevier Oceanography Series, 1996, **61**, 413–452.
6. Chu, P.C.; Ivanov, L.M.; Korzhova, T.P.; Margolina, T.M.; Melnichenko, O.M. Analysis of sparse and noisy ocean current data using flow decomposition. Part 1: Theory. *J. Atmos. Oceanic Technol.* 2003, **20**, 478-491.

Peer-reviewed version available at *Climate* **2019**, *7*, 137; doi:10.3390/cli7120137

7. Chu, P.C.; Ivanov, L.M.; Korzhova, T.P.; Margolina, T.M.; Melnichenko, O.M. Analysis of sparse and noisy ocean current data using flow decomposition. Part 2: Application to Eulerian and Lagrangian data. *J. Atmos. Oceanic Technol.* 2003, **20**, 492-512.
8. Chu, P.C.; Fan, C.W. Accuracy progressive calculation of Lagrangian trajectory from gridded velocity field. *J. Atmos. Oceanic Technol.* 2014, **31**, 1615-1627.
9. Huang N.; Shen, Z.; Long, S.R.; Wu, M.C.; Smith, H. H.; Zheng, Q.; Yen, N.; Tung, C. C.; Liu, H. H. The empirical mode decomposition and the Hilbert spectrum for nonlinear and non-stationary time series analysis, *Proc. R. Soc. Lond* 1998, **454**, 903-995.
10. Chu, P.C.; Fan, C.W.; Huang, N. Compact empirical mode decomposition— an algorithm to reduce mode mixing, end effect, and detrend uncertainty, *Adv. Adaptive Data Anal.* 2012, **4** (3) 1250017 (18 pages) doi: 10.1142/S1793536912500173.
11. Chu, P.C.; Fan, C.W.; Huang, N. Derivative-optimized empirical mode decomposition for the Hilbert-Huang transform, *J. Comput. Appl. Math.* 2014, **259**, 57-64.
12. Qiao, F.L.; Yuan, Y.L.; Deng, J.; Dai, D.J.; Song, Z.Y. Wave-turbulence interaction-induced vertical mixing and its effects in ocean and climate models. *Phil. Trans. R. Soc.* 2016, **A374**: 20150201. http://dx.doi.org/10.1098/rsta.2015.0201.
13. Collins, C.A.; Ivanov, L.M.; Melnichenko, O.B.; Gartfield, N. California Undercurrent variability and eddy transport estimated from RAFOS float observations. *J. Geophys. Res.* 2004, **109**, C5, doi: 10.1029/2003JC002191.
14. Collins, C.A.; Margolina, T.; Rago, T. A.; Ivanov, L.M. Looping RAFOS floats in the California Current System. Deep-Sea Res. II 2013, **85**, 42-61.